Journal of Applied Polymer Science

Polypropylene random copolymer/MWCNT nanocomposites: Isothermal crystallization kinetics, structural, and morphological interpretations

Pawan Verma, Veena Choudhary
Centre for Polymer Science and Engineering, Indian Institute of Technology Delhi, New Delhi 110016, India
Correspondence to: V. Choudhary (E-mail: veenach@hotmail.com or veenach@polymers.iitd.ac.in)

ABSTRACT: This article describes the crystallization process of polypropylene random copolymer (PPCP) under isothermal conditions in presence of varying amounts of multiwalled carbon nanotubes (MWCNT) ranging from 0.5 to 4.0% w/w. Increase in the crystallization temperature under dynamic conditions confirmed the nucleating behavior of MWCNTs, which was also corroborated by crystallization studies under isothermal conditions. The crystallization kinetics was analyzed using Avrami equation and the parameters such as Avrami exponent, the equilibrium melting temperature and fold surface energy for the crystallization of PPCP chains in nanocomposites were obtained from the calorimetric data in order to determine the effect of MWCNTs on these parameters. Spherulitic growth of PPCP crystals was also investigated as a function of time and MWCNT content using hot stage polarizing microscope.
 J. Appl. Polym. Sci. **2015**, *132*, 41734.

KEYWORDS: composites; crystallization; graphene and fullerenes; kinetics; nanostructured polymers; nanotubes

Received 18 June 2014; accepted 8 November 2014
DOI: 10.1002/app.41734

INTRODUCTION

Copolymerization of propylene with ethylene or other olefins is an impressive way to produce high-impact polypropylene resins without using elastomers.[1–5] Random or block ethylene–propylene copolymer with low ethylene content is commercially valuable because the ethylene improves the impact properties of polypropylene without seriously affecting the other desirable properties. In such copolymers, ethylene sequences also decrease the structural regularity which may also affect the crystallization behavior of polypropylene. Therefore, a comprehensive study of crystallization behavior is essential to optimize the processing parameters, such as mold temperature and holding time, which further help to achieve desired crystal morphology for specific applications at lowest possible processing time. It also helps to understand and control the crystallization behavior of materials. Basically crystallization is a two stage process: nucleation and growth. Usually differential scanning calorimetry (DSC) is used to determine such type of thermophysical properties of polymers whereas Avrami and Hoffman-Lauritzen analysis were used to evaluate the overall crystallization kinetics of polymer. Avrami analysis is based on the assumption that the heat released during crystallization is directly proportional to the relative crystallinity whereas Hoffman-Lauritzen analysis suggests that the nucleation and movement of the macromolecules were controlled by the crystallization in the melt.[6–12]

It is well reported in the literature that the crystallization kinetics of polymer is very much affected by the presence of external materials (filler). The most commonly used fillers include various grades of calcium carbonate, quartz, mica, silica flour, talc, various clays, fibers, and carbon nanotubes (CNTs). Among all, CNTs have become the most important nanofiller for polymer matrix because of its extraordinary thermal, mechanical, optical, and electrical properties.[13–15] Incorporation of CNTs disturbed the overall crystallinity and crystal structure of polymer which reveals the change in properties of resulting composites.[16–18] A number of studies have explained the structure property relationship of CNT/polymer composites in the last few years.[19–21] It has been observed that CNTs act as a nucleating agent which enhances the rate of crystallization and properties of polymer matrix.[22–27] Jin *et al.*[28] reported the effect of modified and unmodified MWCNTs in poly(ethylene oxide). In this study, the number of nucleating sites reduced and the crystal size changed from spherical to disk like. Diez-Pascual *et al.*[29] also reported a decrease in the crystallization temperature of poly(ether ether ketone) upon incorporation of SWCNTs without affecting the melting temperature. Choudhary *et al.* reported that the addition of MWCNTs did not affect the crystallinity of poly(trimethylene terephthalate) (PTT); however, it restricted the spherulitic growth of PTT under isothermal and nonisothermal crystallization process.[30]

In spite of extensive investigations, the effect of CNTs on thermal properties especially crystallization kinetics and crystal morphology is still not fully understood as it varies from one polymer matrix to the other. However, understanding of crystallization kinetics of polymers in the presence of CNTs are very interesting for extending their applications, as thermal, optical, and mechanical properties of such composites depend on their morphology, crystal structure, and degree of crystallinity. These composites can further use for electromagnetic shielding application. Thus, understanding the crystallization behavior of polymer in the presence of filler will help in optimizing the processing conditions to achieve the desired crystal morphology for specific applications. Although crystallization kinetics of PP has been well studied in the presence of different fillers,[8,31–38] however to the best of our knowledge, no report is available on the isothermal crystallization kinetics of polypropylene random copolymer (PPCP) in the presence of MWCNTs. Since crystallization kinetics depend not only on the filler characteristics but also on the nature of matrix; therefore, it was considered of interest to investigate the crystallization kinetics of PPCP in presence of varying amounts of MWCNTs under isothermal conditions.

EXPERIMENTAL

Materials

PPCP is a polypropylene with ethylene content. PPCP (Repol R120MK from Reliance Industries) having melt flow index 12 g/10 min (230°C/2.16 kg) and ethylene content of 3–3.5% w/w was used as matrix.

Multiwalled carbon nanotubes (MWCNTs) were synthesized by using chemical vapor deposition (CVD) method using the procedure described by Mathur *et al.*[39] The purity of MWCNTs was determined by recording thermogravimetric trace in oxygen atmosphere which was ~96%. Char yield obtained was about 4% as an impurity of iron catalyst or its oxides present in the sample. The morphological characterization done using scanning electron microscopy (SEM) and transmission electron microscopy (TEM) confirmed that CNTs are multiwalled with inner and outer diameter varying from 10 to 12 nm and 30 to 40 nm, respectively, and a length of ~ 20–40 μm. Room temperature Raman scattering of MWCNTs revealed the tangential band at 1580 cm^{-1} (*G* band) and the disorder induced band at 1352 cm^{-1} (*D* band). The ratio of *D* band to *G* band peak was used to find out the amount of disorder within nanotubes which was found to be 0.24. As reported in the literature, a small I_D/I_G ratio (0.1–0.2) indicates that the defect level in the atomic carbon structure is low, which suggests reasonable crystalline quality. These studies clearly show that the MWCNTs synthesized in the present work has very few defect structures.[40]

Preparation of PPCP/MWCNTs Nanocomposites by Melt Compounding

PPCP/MWCNTs nanocomposites were prepared by melt blending using corotating HAAKE MiniLab II microcompounder with processing temperature 200°C, mixing time ~10 min, and screw speed ~50 rpm. Before compounding, the nanotubes and PPCP copolymer were dried at 80°C for 6 h. PPCP/MWCNT nanocomposites were prepared by mixing PPCP with 0, 0.5, 1.0, 2.0, and 4.0% w/w of MWCNTs in a tumbler before compounding. The samples have been designated as PPCP-0, PPCP-0.5, PPCP-1, PPCP-2, and PPCP-4 where PPCP represents the copolymer and numerals represent the weight percent of MWCNTs. For example, PPCP nanocomposites prepared by mixing 0, 0.5, and 1% w/w of MWCNT have been designated as PPCP-0, PPCP-0.5, and PPCP-1, respectively.

Characterization of Nanocomposites

Morphological Characterization. Surface morphology of nanocomposites was investigated by using SEM (EVO-50) operated at an accelerating voltage of 20 kV. For this purpose, cryogenically fractured samples were used. The samples were coated first with silver. A thin film of gold, applied using sputtering or vacuum evaporation, delivers an excellent conformal conductive coating for scanning purpose. Coating helps to promote the emission of secondary electrons and to prevent charging of the surface.

Differential Scanning Calorimetry. DSC, Model Q200TA was used for recording DSC scans (heating and cooling) under nitrogen atmosphere for isothermal and nonisothermal crystallization studies. For recording DSC scans, sample (5 ± 1 mg) was heated at a rate of 10°C/min under N_2 atmosphere using aluminum crucible. The sample was first heated from room temperature to 200°C and then held at this temperature for 3 min to remove the thermal history and then cooled to room temperature at a cooling rate of 10°C/min. In the cooling scan, an exotherm due to crystallization was observed. The second heating scans recorded at a heating rate of 10°C/min were used for determining the melting point of polymer.

To examine the crystallization behavior of PPCP and PPCP/MWCNT nanocomposite samples under isothermal conditions, the samples were heated from room temperature to 200°C at a heating rate of 10°C/min, held at that temperature for 2 min to remove the thermal history and then rapidly quenched to the predetermined crystallization temperatures 115, 120, 125, and 130°C. For this analysis, DSC scans were recorded as a function of time till complete crystallization followed by recording the heating scan at a heating rate of 10°C/min for recording melting endotherm.

Polarized Light Microscopy. To investigate the nature of spherulitic growth, size of spherulites, and crystal morphology, hot stage polarizing microscope (Meize Techno, Japan) was used. The microscope has a camera of 12 mega pixel resolution with a maximum magnification of 20×. Thin-film samples were prepared by melting on a glass slide at 200°C with a piece of cover glass and held for 2 min to eliminate previous thermal history. The samples were then quickly cooled to the predetermined crystallization temperature. The crystallite growth was recorded by a video camera as a function of time and CNT content.

Wide-Angle X-ray Diffraction. Wide-angle X-ray diffraction (WXRD) patterns were recorded on a PANatytical instrument, model number PW3040/60 X'pert Pro (Netherlands) with Ni filtered CuK_α radiation ($\lambda = 0.154$ nm) under a current and a voltage of 30 mA and 40 kV, respectively. The samples were scanned from $2\theta = 5°–60°$ at a rate 2°/min. Injection molded samples were used for this analysis.

RESULTS AND DISCUSSION

Surface Morphology of Nanocomposites

SEM micrographs of PPCP and PPCP/ MWCNT nanocomposites are depicted in Figure 1. These images evidently show a uniform distribution of CNTs in all the samples which confirms that melt blending is an efficient technique for the preparation of nanocomposites. In SEM image of sample having 1 wt % of CNT (PPCP-1) [Figure 1(b)], an interesting phenomenon of alignment was observed. Some of the CNT bundles pulled out from the matrix are also seen in the images suggesting the lack of compatibility between CNTs and polymer matrix.

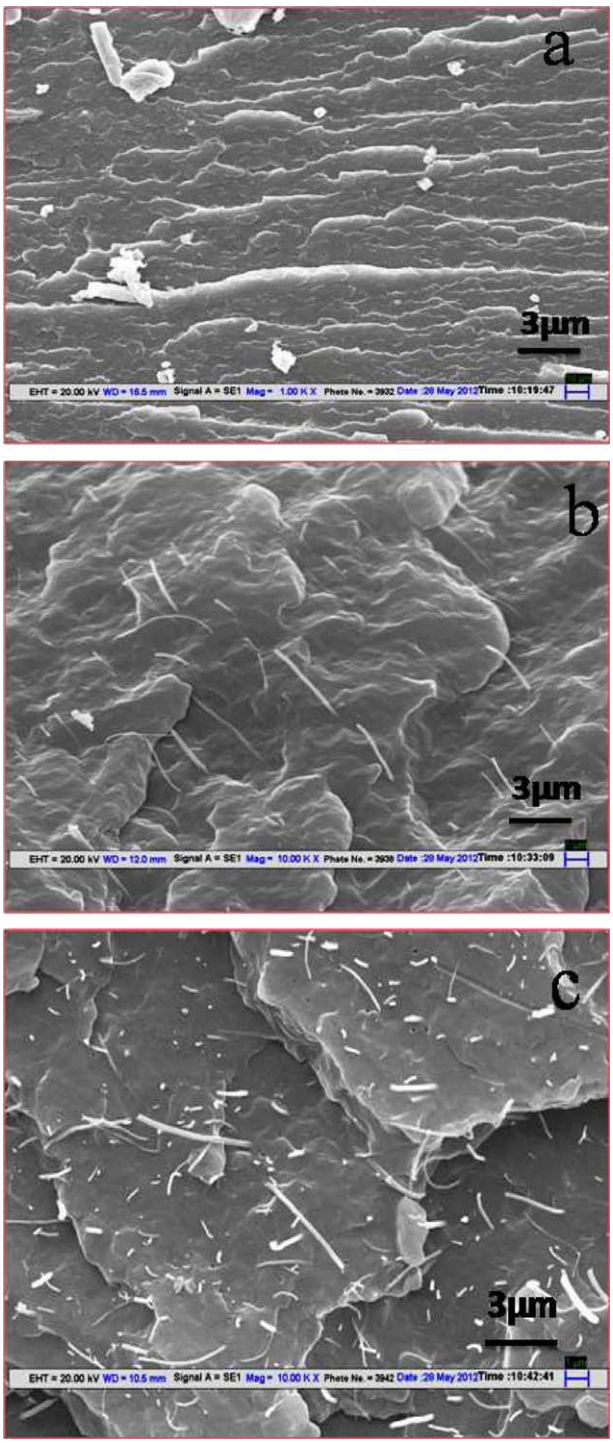

Figure 1. SEM images of PPCP/MWCNT nanocomposites: (a) PPCP-0, (b) PPCP-1, and (c) PPCP-4. [Color figure can be viewed in the online issue, which is available at wileyonlinelibrary.com.]

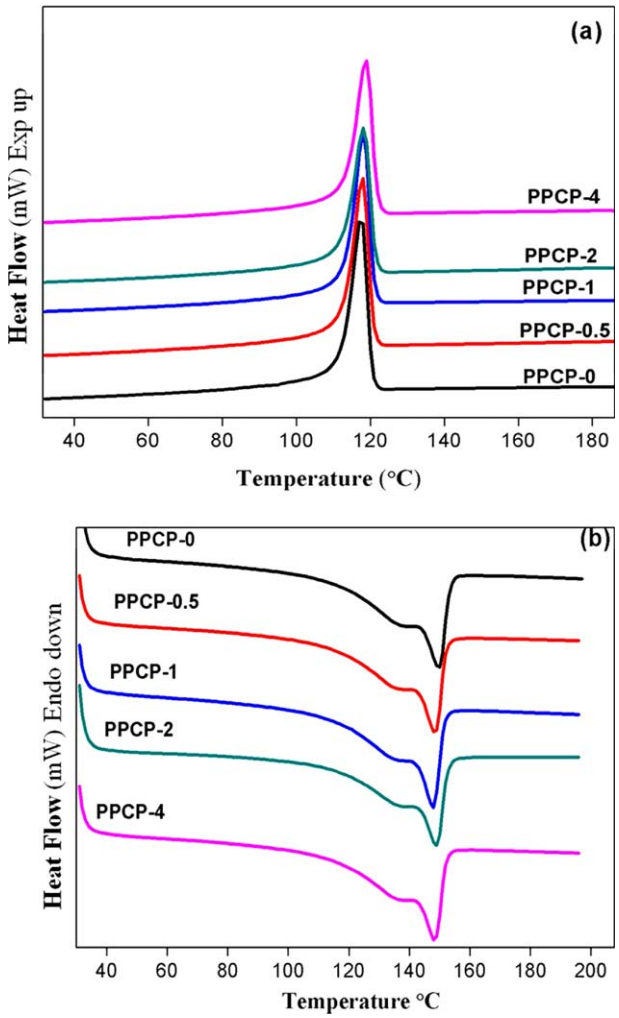

Figure 2. DSC scans of PPCP and PPCP/MWCNT nanocomposites (a) cooling and (b) heating scans. [Color figure can be viewed in the online issue, which is available at wileyonlinelibrary.com.]

DSC Analysis

Figure 2(a,b) shows the DSC cooling and heating traces, respectively, of PPCP and its nanocomposites having varying amounts of MWCNTs. In the cooling scan [Figure 2(a)], an exothermic transition due to crystallization was observed in all the samples. The crystallization exotherm was analyzed by noting the following characteristics:

T_{onset}: onset temperature of crystallization;

T_c : peak exotherm temperature;

ΔH_c heat of crystallization.

The results of cooling exotherm summarized in Table I showed that the onset of crystallization temperature (T_{onset}) of PPCP increased by ~4°C at a loading of 0.5 wt % CNT (PPCP-0.5).

Table I. Results of DSC Scans: Effect of MWCNTs on Crystallization and Melting Behavior of PPCP

Sample designation	Tonset (°C)	Tc (°C)	ΔHc (J/g)	Tm2	ΔT = Tm2 –Tc
PPCP-0	120.60	116.0	75.15	149.6	33.06
PPCP-0.5	124.52	117.8	75.96	149.4	31.65
PPCP-1	124.18	118.1	76.07	148.8	30.71
PPCP-2	124.68	118.1	76.67	149.8	31.76
PPCP-4	124.47	118.9	79.62	149.2	30.30

T_{onset}, onset temperature of crystallization; T_c, peak exotherm temperature; ΔH_c, heat of crystallization from the area under the exothermic peak; T_{m2}, peak endothermic temperature/melting temperature; ΔT = Super cooling temperature [$T_{m2} - T_c$].

Further increase of MWCNTs did not show much affect on T_{onset}. The peak exotherm temperature (T_c) showed an increase of ~3°C at a loading of 4 wt % MWCNTs (PPCP-4). The increase in T_c confirms the nucleating effect of MWCNTs which was further supported by the super cooled temperature (ΔT). The peak exotherm temperature and peak temperature of melting endotherm (T_{m2}) was used to calculate $\Delta T = (T_{m2} - T_c)$. The T_{m2} did not show much change upon incorporation of varying amounts of MWCNTs (Table I); however, ΔT showed a decrease thereby confirming that MWCNTs act as nucleating agent. Similar behavior has been reported for PTT[41,42] where ΔT is inversely proportional to MWCNTs loading.

The second heating scans [Figure 2(b)] were used to evaluate the melting characteristics of PPCP in the absence and presence of varying amounts of MWCNTs. In the second heating scan, two melting endotherms were observed for each sample. The appearance of double fusion endotherms could be either because of previous crystallization conditions (cooling rate) or melting of different lamellar crystals and presence of different crystallite size.[43] Another explanation for the double melting behavior could be due to the step-like melting mechanism proposed by Rodriguez *et al.*[44] They reported that the second melting endotherm could be due to the combination of melting of two population one consisting of reversing primary crystals and the other consisting of nonreversing primary crystals. The endothermic peak temperatures noted as T_{m1} and T_{m2} did not show any significant change upon incorporation of varying amounts of MWCNTs; however, peak broadening was observed and onset of melting starts at much lower temperature. About 10°C decrease in the onset of melting was observed at a loading of 4% MWCNT (PPCP-4) in first endotherm. The decrease in onset of melting confirms the formation of imperfect crystals in the presence of MWCNTs. From the area under the endothermic transition, heat of fusion was calculated which was used to determine the percent crystallinity using eq. (1):

$$X_c = (\Delta H_f / \Delta H_{fo}(1 - X_p)) \times 100 \quad (1)$$

where ΔH_f is the melting enthalpy of sample (J/g). $\Delta H_{fo} = 207$ J/g for PP (from the literature). X_p = weight fraction of filler.

Since specific value of ΔH_{fo} for PPCP does not exist, for this study the enthalpy of fusion for 100% crystalline polypropylene was used, i.e., 207 J/g because fusion enthalpy is almost independent of isotacticity. The same value has also been used for the calculation of % crystallinity of PPCP nanocomposites by Sahin *et al.*[45] Percent crystallinity of nanocomposites increased slightly with MWCNTs loading. The results of melting and % crystallinity are summarized in Table II.

Isothermal Crystallization Kinetics

Estimation of isothermal crystallization parameter is normally carried out using the data obtained from crystallization exotherm with a basic assumption that heat released during crystallization is directly proportional to the relative crystallinity. On the basis of this assumption, the relative crystallinity X_t, was determined as the ratio of the exothermic peak area at time t and that at infinite time, using the following eq. (2):[46]

$$X_t{}^t = \frac{\int_0^t \frac{dH}{dt} \cdot dt}{\int_0^\infty \frac{dH}{dt} \cdot dt} = \frac{\Delta H_t}{\Delta H_\infty} \quad (2)$$

where dH/dt represents the heat of evolution; ΔH_t is the heat evolved at time "t"; ΔH_∞ is the total heat evolved during the complete crystallization process.

The isothermal crystallinity of PPCP and its nanocomposites was analyzed in terms of Avrami equation which is as follows:

Table II. Results of DSC Scans (Heating): Effect of MWCNT Content on Melting Behavior and Percent Crystallinity of PPCP and PPCP/MWCNT Nanocomposites

Sample designation	First endotherm (°C)		Second endotherm (°C)		ΔH_f (J/g)	% Crystallinity (from DSC)	% Crystallinity (from XRD)
	T_{onset}	T_{m1}	T_{onset}	T_{m2}			
PPCP-0	96.03	136.5	143	149.6	75.85	36.64	43.0
PPCP-0.5	94.03	135.7	141.7	149.4	76.66	36.86	42.0
PPCP-1	91.14	134.3	140.7	148.8	77.52	37.45	39.6
PPCP-2	87.70	134.0	141.0	149.8	78.17	37.75	45.0
PPCP-4	86.40	135.0	140.7	149.2	80.03	38.82	45.0

T_{onset}= onset *temperature of melting;* T_{m1}, T_{m2} =*endothermic peak temperature/melting temperature;* ΔH_f = *Heat of fusion [determined from the area under the melting endotherm].*

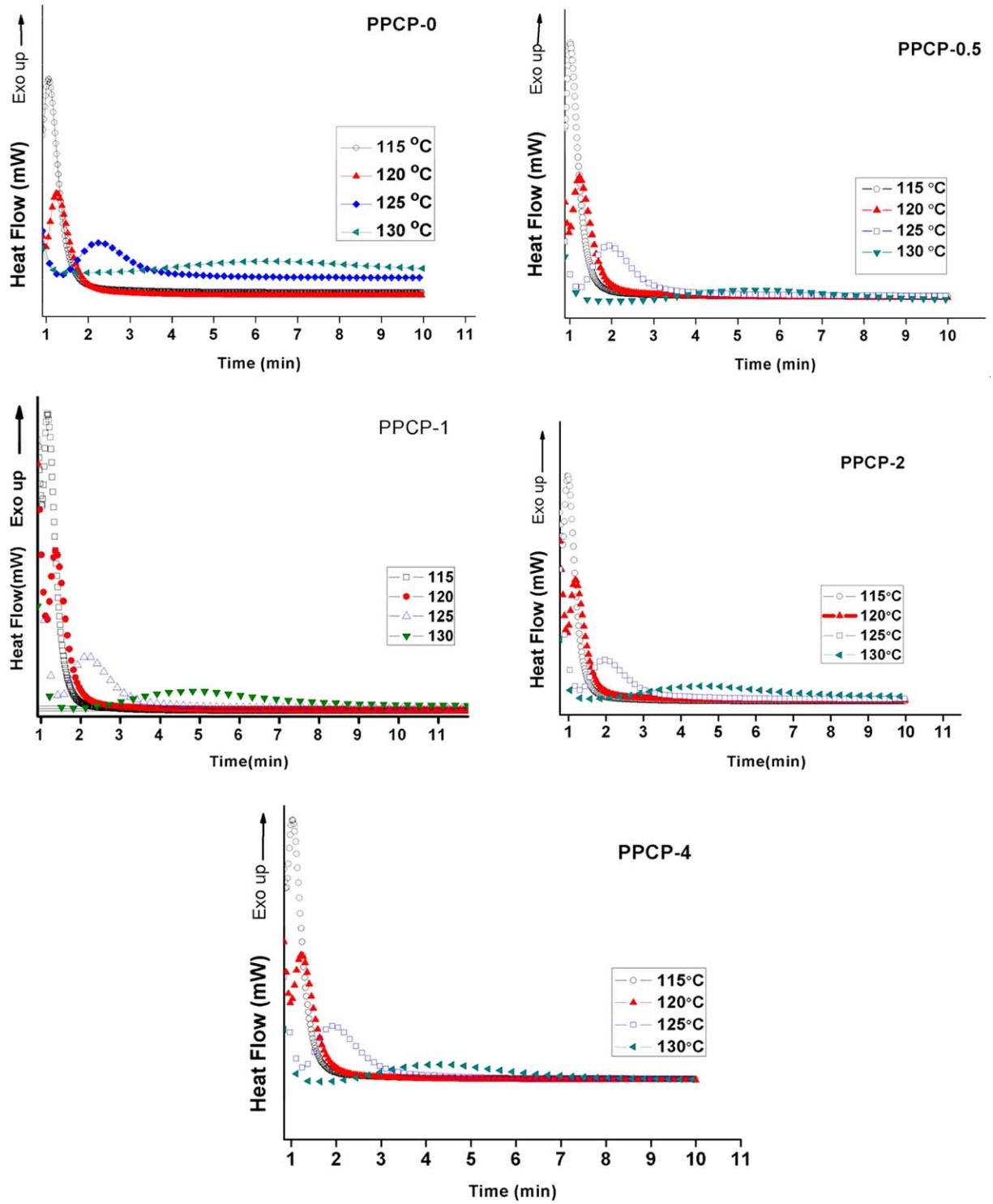

Figure 3. DSC scans recorded under isothermal conditions for PPCP and its nanocomposites. [Color figure can be viewed in the online issue, which is available at wileyonlinelibrary.com.]

$$1-X_t=\exp\left(-kt^n\right) \quad (3)$$

where n is the Avrami exponent and its value depends on the mechanism of nucleation and type of crystal growth; k is the Avrami rate constant or crystallization rate constant involving both nucleation and growth rate parameter; and X_t is the relative crystallinity at time t.

Figure 3 shows the isothermal crystallization exotherms for neat PPCP and PPCP/MWCNT nanocomposites containing 0, 0.5, 1, 2, and 4 wt % MWCNTs (i.e., samples PPCP-0, PPCP 0.5, PPCP-1, PPCP-2, and PPCP-4). From the graphs, it is clear that as the isothermal crystallization temperature increased, the time required for complete crystallization also increased in all the

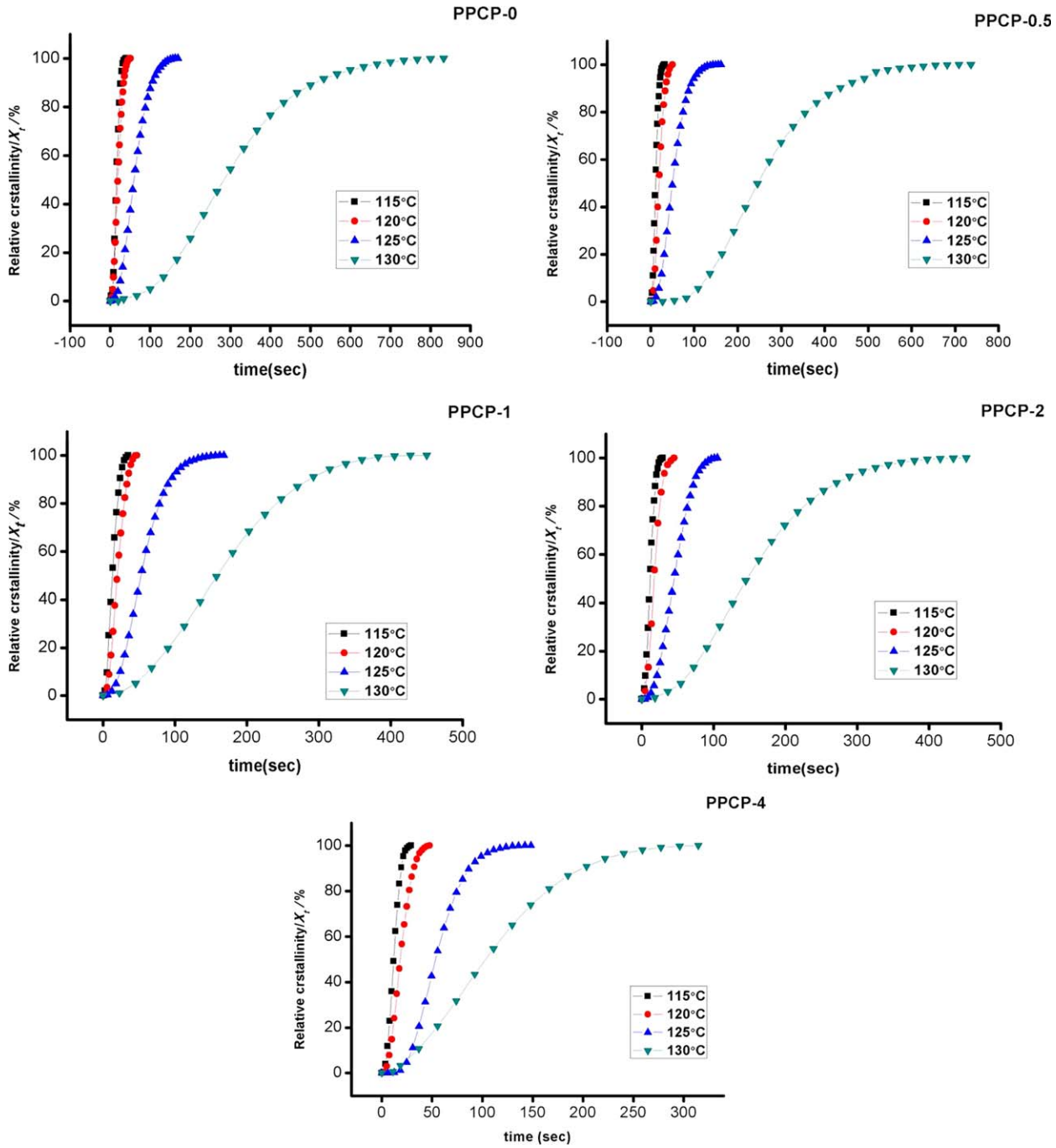

Figure 4. Plot of relative percent crystallinity versus time for neat PPCP and PPCP/MWCNT nanocomposites. [Color figure can be viewed in the online issue, which is available at wileyonlinelibrary.com.]

samples. On the other hand, the time required for complete crystallization decreased with the incorporation of varying amounts of MWCNTs which reveals that presence of MWCNTs speed up the crystallization process.

Figure 4 shows the change in relative crystallinity with respect to time for PPCP and PPCP/MWCNTs nanocomposites (i.e., samples PPCP-0, PPCP 0.5, PPCP-1, PPCP-2, and PPCP-4) at different crystallization temperatures which exhibited a decrease in crystallization time at any given temperature in the presence of MWCNTs. All curves are showing similar sigmoidal shape and shifted to the right as the isothermal crystallization temperature increased. Half-time of crystallization ($t_{1/2}$) can also be determined directly from the sigmoidal shape curve which is defined as the time required for the completion of 50% crystallization and the results are summarized in Table III.

In order to find out the value of n and k, eq. (3) was simplified by taking double logarithmic linear form as shown in eq. (4). The value of n and k can be obtained directly from the slope

Table III. Values of *n*, *k*, *k′*, $t_{1/2}$, and *G* Obtained from the Cooling Exotherms

Samples designation	Isothermal crystallization temperature (°C)	n	k × 105 (s−n)	k′ × 105 (s−n)	t1/2 (min)	1/t1/2 = G (min−1)
	115	2.33	110	105	0.27	3.70
PPCP-0	120	2.42	50.5	54.4	0.32	3.12
	125	2.32	4.90	5.44	0.98	1.02
	130	2.14	0.30	0.38	4.76	0.21
	115	2.36	200	105	0.26	3.84
PPCP-0.5	120	2.44	43	44.4	0.35	2.85
	125	2.37	5.48	4.44	0.98	1.01
	130	2.78	0.01	0.01	4.72	0.21
	115	2.14	276	306	0.21	4.76
PPCP-1	120	2.35	62.9	5.1	0.33	3.03
	125	2.26	7.63	1.12	0.87	1.14
	130	2.13	1.46	5.64	2.66	0.37
	115	2.57	121	133	0.19	5.26
PPCP-2	120	2.25	112	112	0.29	3.44
	125	2.63	3.07	3.0	0.76	1.31
	130	2.13	1.5	1.6	2.45	0.40
	115	2.61	102	120	0.19	5.26
PPCP-4	120	2.36	66	75	0.30	3.33
	125	3.10	0.02	0.02	0.90	1.11
	130	1.94	8.6	8.3	1.75	0.57

and intercept of the best fitted lines of the plot of ln [−ln $(1 - X_t)$] versus ln *t*, where *k* and *n* are used to describe the crystalline morphology and type of nucleation[56]:

$$\ln\ [-\ln\ (1-X_t)]=\ln k+n\ \ln t. \quad (4)$$

Figure 5 shows the plots of ln[−ln$(1 - X_t)$] versus ln*t* for neat PPCP and PPCP/MWCNT nanocomposites. We observed here that the plots are linear in the beginning (at low relative crystallinity) and the deviation from linearity observed at higher relative crystallinity is attributed to the fact that Avrami equation can be applied to describe the beginning of isothermal crystallization, i.e., under 25% crystallinity. The deviation from linearity could also be due to the secondary crystallization.[47] The values of *n*, *k*, $t_{1/2}$, and *G* (growth rate) obtained from the cooling exotherms of PPCP/MWCNT nanocomposites at different crystallization temperatures are summarized in Table III. The value of *k* was also calculated from half-life ($t_{1/2}$) designated as *k′* with the help of eq. (5)[48] and the results are given in Table III.

$$k=\ln 2/t_{0.5}^{n}. \quad (5)$$

The value of *k* obtained by two different methods showed a good agreement at higher crystallization temperature. The crystallization rate constant, *k*, decreased with increasing crystallization temperature, indicating that the rate of the three dimensional crystallization growth was reduced by increasing the crystallization temperature.[49] However, there is no definite trend on incorporation of MWCNTs. At 130°C, The value of *k* varied from 0.3×10^{-5} for PPCP, to 8.6×10^{-5} for PPCP-4, i.e., PPCP having 4% by weight of MWCNT, indicating the nucleating behavior of MWCNT on PPCP matrix under isothermal conditions. Similar behavior has also been reported by Carlos *et al.*[50] According to the nucleation growth mechanism, the value of *n* should be an integer, but here we are getting the noninteger values ranging from 1.94 to 3.10. These noninteger values are caused by mixed growth and/or surface nucleation modes and two-stage crystallization. The value of n reported in the literature ranges from 1.8 to 4[49] for different systems. The value of *n* represents the dimensional growth of crystal. The *n* value (2.14–2.42) of PPCP and PPCP nanocomposites showed two-/or three-dimensional heterogeneous crystal growth which changes with composition. In case of sample having 4 wt % MWCNT, i.e., PPCP-4, value of *n* is less than 2 at crystallization temperature of 130°C indicating two dimensional hindered crystal growths. The $t_{1/2}$ which is used to characterize the rate of crystallization; higher half time ($t_{1/2}$) lower the crystallization rate. The $t_{1/2}$ values are reported in Table III increased with increasing T_c and deceased with MWCNT content. The increase in $t_{1/2}$ with increasing crystallization temperature indicated that higher the crystallization temperature higher the time required for complete crystallization while on other hand with MWCNT loading the rate of crystallization for PPCP/MWCNT nanocomposites was faster than neat PPCP because half time value is decreasing with MWCNT loading. It reveals that MWCNTs act as the nucleating agent that accelerates the crystallization of PPCP in the composites.

Secondary Nucleation Theory

Secondary nucleation theory of Hoffman and Lauritzen suggest that the overall crystallization rate should be controlled by nucleation and transport of macromolecules in melt.[8,51] This

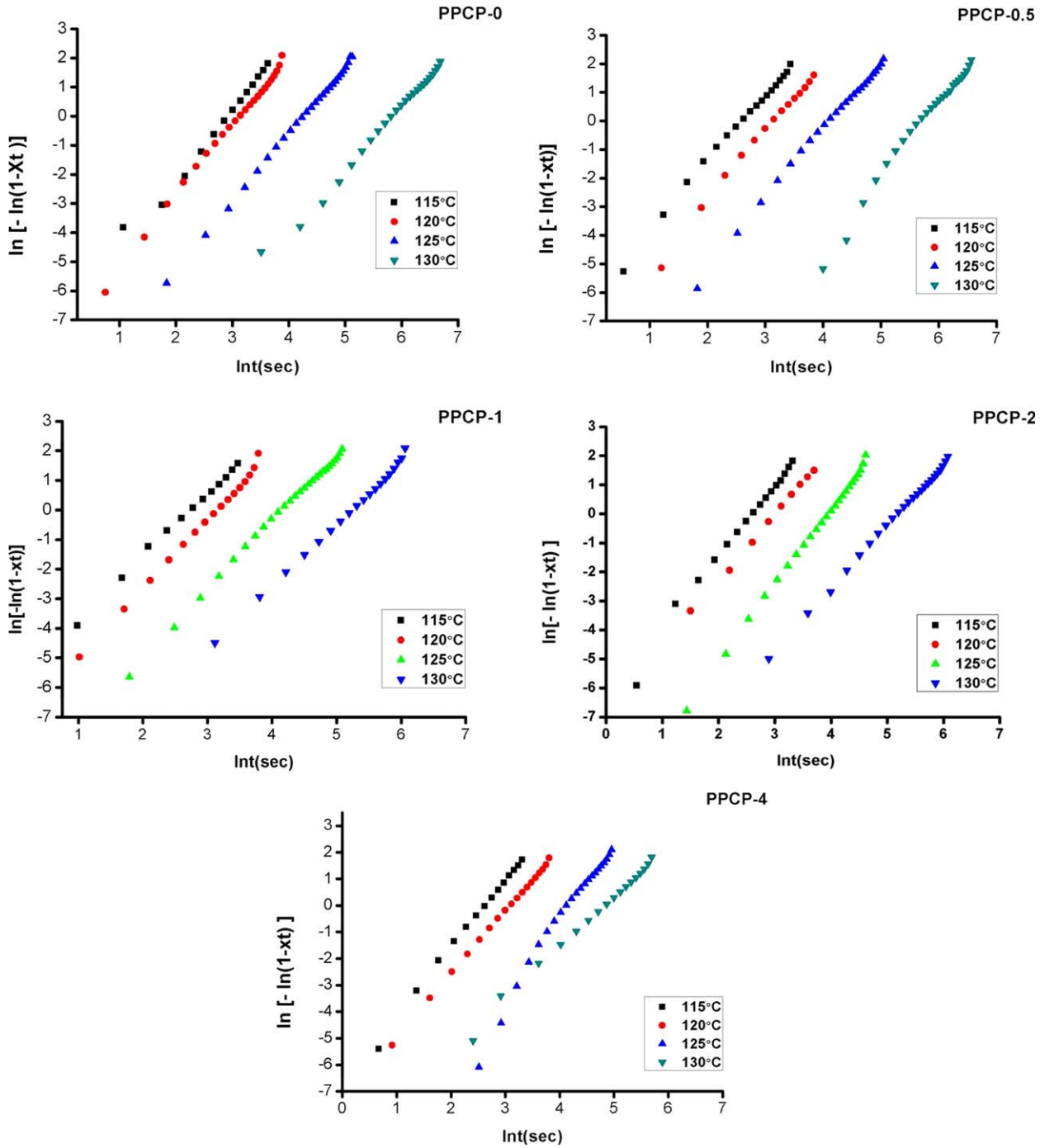

Figure 5. Plots of ln[-ln(1 − X_t)] versus lnt for neat PPCP and PPCP/MWCNT nanocomposites. [Color figure can be viewed in the online issue, which is available at wileyonlinelibrary.com.]

theory was used to analyze the nucleating effect of MWCNTs on crystallization of PPCP According to Hoffman–Lauritzen theory, the temperature dependence of the linear growth rate of PPCP can be represented by eq. (6):

$$G = G_o \exp\left(\frac{-U^*}{R\,(T_c - T_\infty)}\right) \exp\left(\frac{-K_g}{T_c\;\Delta T\;f}\right). \qquad (6)$$

where G_0 is a constant independent of temperature, U^* is the activation energy related to the short diffusion distance of the crystalline unit across the phase boundary G is the linear growth rate, K_g is the nucleation parameter, R is the gas constant, T_c is the crystallization temperature, T_∞ is the hypothetical temperature where crystallization process completed and below which no chain mobility; $T_\infty = T_g$ – 30K where $T_g = 240$ K and $U^* = 6280$ J/mol, $R = 8.32$ Jmol^{-1}K^{-1}. In addition, f is a corrective factor given as $f = 2\;T_c/\;(T_c - T_m^o)$ and ΔT is the degree of undercooling defined by $\Delta T = T_m^o - T_c$ where T_m^o is the equilibrium melting temperature. Here, we are taking

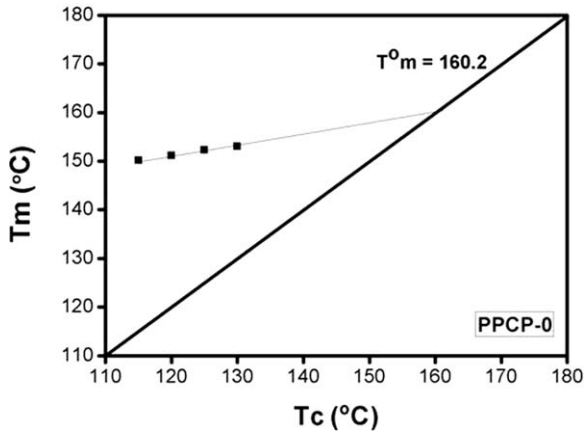

Figure 6. Determination of equilibrium melting temperature for PPCP using linear Hoffman-Weeks equation.

$T_m^o = 176.4°C$ (determined from nonlinear Hoffmann–Weeks equation mentioned below), for calculation purpose.

To find out the equilibrium melting temperature, the PPCP samples after complete crystallization at different isothermal temperature, (i.e., 115, 120, 125, and 130°C) were heated at a rate of 10°C/min upto 190°C and the melting endotherms were recorded.

Wu *et al.*[52] reported that the equilibrium melting temperature (T_m^o) for a semicrystalline polymer could be determined via four general methods including the Gibbs–Thomson[51] and Flory–Vrij [53] approaches, the H–W procedure,[54] and the fitting of growth-rate data at a sufficiently low under cooling with the classical theory of lamellar crystal growth.[55] Among all the approaches, the H–W analysis has been usually used to estimate the T_m^o value because of the simplicity which involves the use of experimental values. The H–W method is further divided into linear and non-linear Hoffman-Weeks method. In linear procedure, the measured T_m's of samples crystallized at different T_c were plotted against T_c and a linear extrapolation to the line $T_m = T_c$, where the intercept gaveT_m^o. Although this approach was not developed to provide the best estimate of T_m^o, yet it is used to explain the observed rise in the melting temperature with T_c.[56] The plot of T_m versus T_c showed a linear relationship and the H–W extrapolation was carried out according to the following equation. The linear H–W extrapolation is carried out and one may obtain an extrapolation temperature according to eq. (7):

$$T_m = T_m^o 1 - 1/r) + T_c/r. \quad (7)$$

Where T_m^o is the equilibrium melting temperature and $r = l/l^*$ is the ratio of lamellar thickness l at the time of melting to the thickness l^* of the critical nucleus at T_c. From Figure 6, the value of T_m^o obtained was 160.2°C.

According to Marand and coworkers[52,57,58] in nonlinear H–W method, the scaled melting temperature $M = T_m^o/T_m^o - T_m$ was plotted against the scaled crystallization temperature $X = T_m^o/T_m^o - T_c$ for several choices of T_m^o and the slope should yield a constant lamellar-thickening coefficient (r). For a set of experimental T_m and T_c values, corresponding sets of M, X values can be determined for a given choice of T_m^o value (Figure 7). When this method is used to the melting of existing crystals ($r = 1$), a plot of M versus X should yield a straight line with the slope unity for the actual equilibrium melting temperature (if the interfacial free energy of basal faces for original as well as fully grown crystal is same).

The linear H–W plot of melting temperature at zero crystallinity against T_c revealed the equilibrium melting temperature to be 160.2°C for neat PPCP. By comparison, the nonlinear H–W treatment (linear MX plot) was also carried out and higher equilibrium melting temperature was obtained, i.e., 176.4°C. Similar results have also been reported by Wu *et al.*[52] for PTT. In the study they concluded that the estimation of T_m^o was more sensible if the non-linear H–W method is applied. Therefore, in the present work, the value of T_m^o obtained using nonlinear Hoffmann-Week extrapolation, i.e., 176.4°C was used to find out the degree of super cooling for secondary nucleation theory.

Another kinetic parameter, i.e., K_g is the energy required for the formation of nuclei of critical size and was determined using eq. (8):

$$K_g = \frac{nb\sigma\sigma_e T_m^o}{\Delta H_f k_B}. \quad (8)$$

Where b is the surface nucleus thickness, σ and σ_e are the side surface (lateral) and fold surface free energies which reflect the work required to create a new surface, T_m^o is the equilibrium melting temperature and k_B is the Boltzmann's constant 1.38×10^{-16} ergK^{-1}, ΔH_f is the heat of fusion per unit volume of crystal. The interfacial free energy σ can be given by the following equation.

$$\sigma = \alpha.\ \Delta H_f.(ab)^{1/2} \quad (9)$$

where α is an empirical constant usually assumed to be 0.1, $a = 4.672$ Å, molecular layer thickness, $b = 6.266$ Å and $\Delta H_f = 207$ Jg^{-1} (100% crystalline PP taken from literature). σ can be calculated from eq. (9) and it was found to be 15.0 erg cm^2.[59] Typically, the value of $n = 4$ in regime I or III and $n = 2$

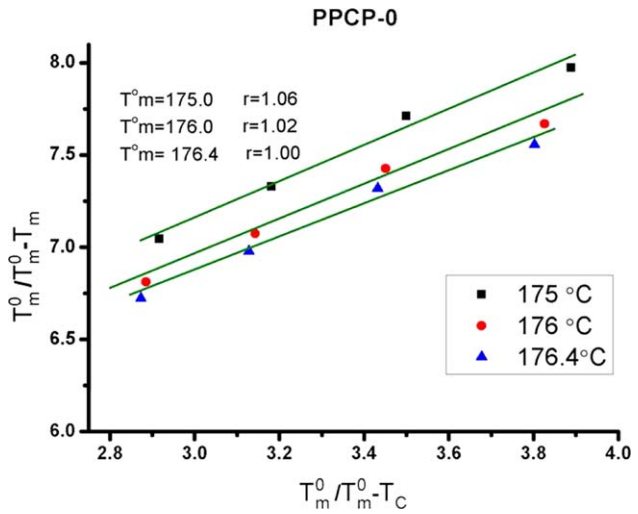

Figure 7. Determination of equilibrium melting temperature for PPCP using nonlinear Hoffman-Weeks equation. [Color figure can be viewed in the online issue, which is available at wileyonlinelibrary.com.]

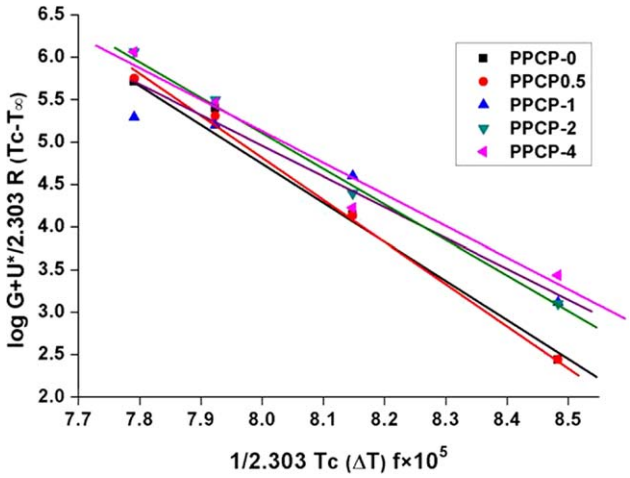

Figure 8. Plot of log $G+U^*/2.303\ R\ (T_c-T_\infty)$ as a function of $1/2.303\ T_c(\Delta T)\ f\times 10^5$. [Color figure can be viewed in the online issue, which is available at wileyonlinelibrary.com.]

in regime II have been employed.[12] Equation (6) can be rearranged as:

$$\log G+\frac{U^*}{2.303\ (T_c-T_\infty)}=\log G_o-\frac{K_g}{2.303\ T_c(\Delta T)f}. \qquad (10)$$

It is known that the primary nucleation rate and the crystal growth rate are related to these crystallization rate parameters Therefore, $1/t_{1/2}$ can be used instead of G. By plotting the log $G+U*/2.303(T_c-T_\infty)$ versus $1/2.303T_c\ (\Delta T)f$, the value of K_g [i.e., $K_g=-$(slope) (Figure 8)] can be determined.

The value of fold surface free energy σ_e can be calculated using eq. (8) with the help of K_g and σ and the obtained values of σ_e and K_g are tabulated in Table IV.

The lower values of K_g and σ_e for nanocomposites reveals that the energy required for the formation of nuclei as well as new surface reduced from neat PPCP which further suggested that the presence of MWCNTs decreased the activation energy of nucleation. It is well known that the addition of filler particles provides a new surface for crystal growth and also reduces nucleus size needed for crystal growth. In this process, the heterogeneity of the system increased, during heterogeneous nucleation, polymeric chains start growing on these pre-existing surfaces and reduce the free energy required for primary nucleation.[11,60] From these results, it can be concluded that the MWCNT act as nucleating agent for PPCP. The n values from Avrami analysis also verify the growth of heterogeneous crystals

Table IV. Lauritzen-Hoffman Parameters for Isothermal Crystallization of PPCP and PPCP/MWCNT Nanocomposites

Sample designation	K_g ($\times 10^5$)/deg^2	σ/erg cm^{-2}
PPCP-0	4.72	92.1
PPCP-0.5	4.5	80
PPCP-1	3.59	81
PPCP-2	4.1	74.3
PPCP-4	3.8	71

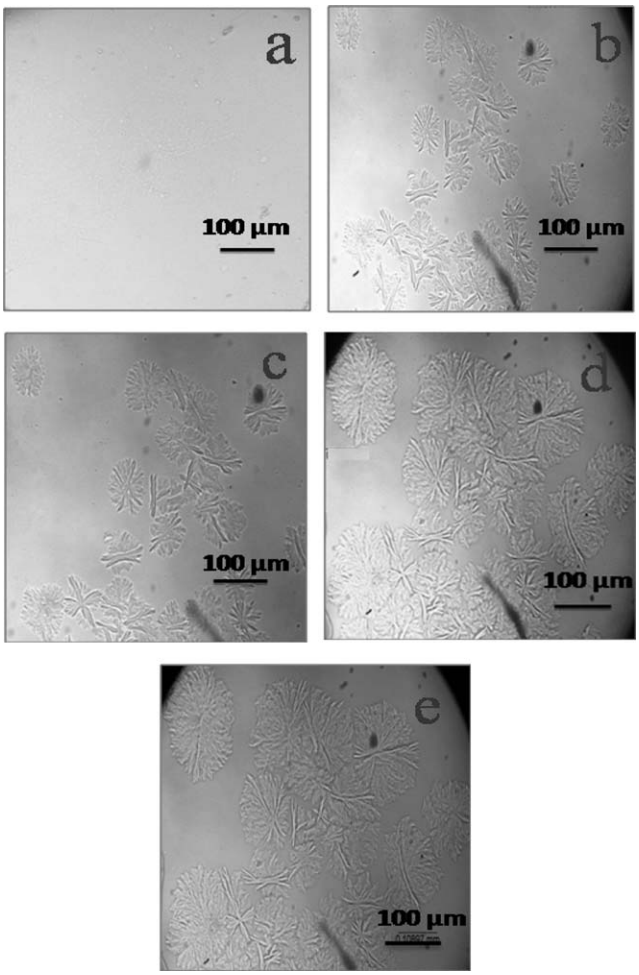

Figure 9. XRD patterns of MWCNT, PPCP, and PPCP/MWCNTs nanocomposites.

while $t_{1/2}$ and ΔT have also supported the nucleating behavior of MWCNT. The nucleating ability of MWCNT reduced energy which is required to create a new surface for crystallization. This in turn also leads to faster crystallization. Another feasible reason could be that the addition of CNTs decreased the free volume, and thus reduced molecular chain mobility, leading to lower K_g and σ_e values. At a given U^*, the values of K_g (4.72×10^5 deg^2) and σ_e (92.1erg cm^{-2}) calculated for neat PPCP agree well with the values reported for isotactic PP.[59]

Crystal Morphology of Nanocomposites

Growth of spherulites of PPCP and PPCP/MWCNT nanocomposites was observed using polarized light microscopy (PLM) and the change in spherulites was observed with respect to time and CNTs content. Figure 9 shows the effect of annealing time on spherulitic growth of neat PPCP which attributed that as the time increased the size of spherulites also increased but after a certain time it became constant. PLM micrographs were taken at an isothermal temperature of 130°C with time interval of 2 min. After 8 min of annealing time, the size of spherulites did not change and the size of spherulites at this moment observed was ≈100 µm. This shows that crystallinity increases with time and longer time was required for complete crystallization at

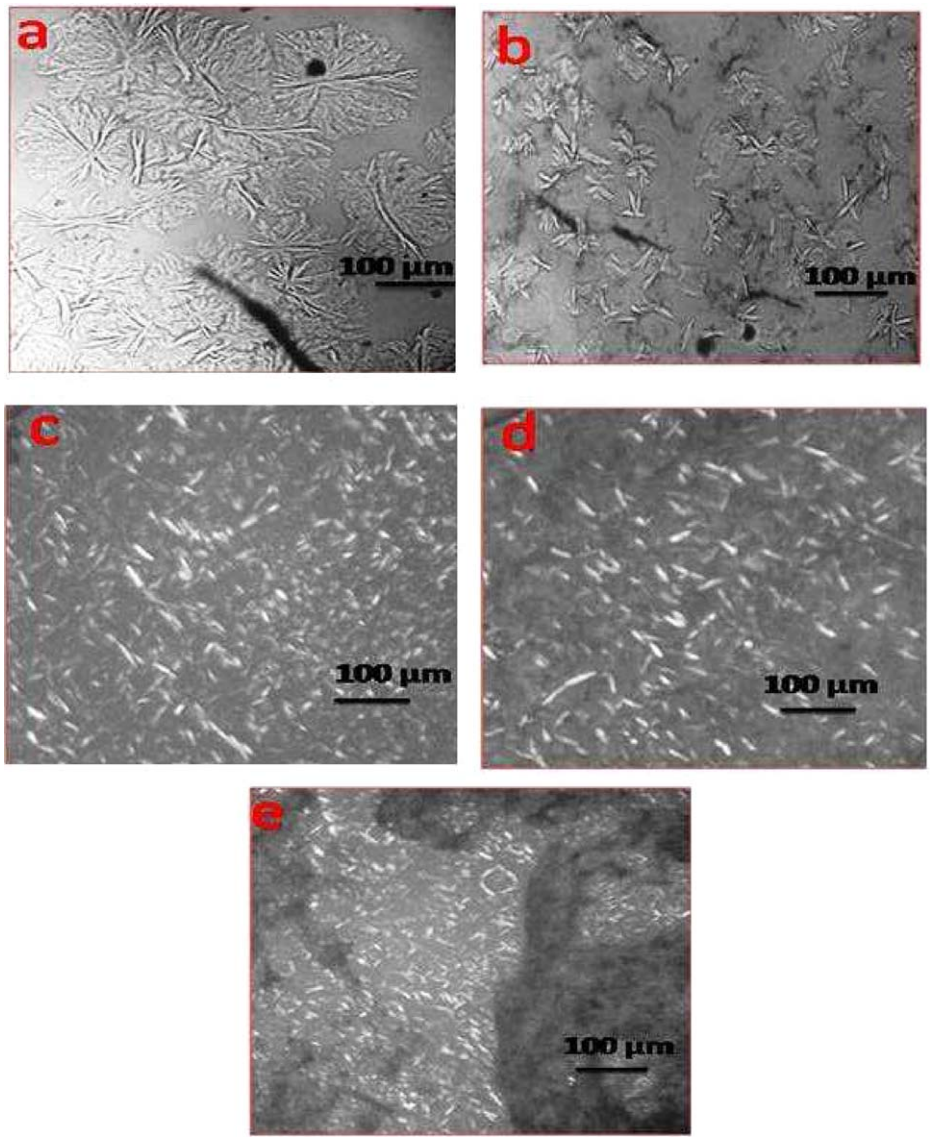

Figure 10. PLM micrographs of PPCP showing effect of annealing time: (a) 0 min, (b) 2.0 min, (c) 4.0 min, (d) 6.0 min, and (e) 8.0 min at 130°C. [Color figure can be viewed in the online issue, which is available at wileyonlinelibrary.com.]

130°C. Higher rate of crystallization was observed at lower isothermal temperature as compared to higher isothermal temperature; therefore, it was difficult to analyze the effect of annealing time at lower crystallization temperature.

Figure 10 shows the effect of CNTs on spherulitic growth which support the results obtained from the isothermal DSC analysis. Incorporation of MWCNTs enhanced the amount of heterogeneous nuclei in PPCP matrix, which is confirmed by Avrami analysis and secondary nucleation theory, resulting in an obvious decrease in spherulites size of PPCP. When the MWCNTs content was 0.5%, the crystals are visible but the growth of crystals hindered due to the presence of MWCNTs. However, when the MWCNTs content increased, only large quantities of small crystal aggregates were visible in the remaining composition (Figure 11). In the last decade, considerable efforts have been made to explain the MWCNTs induced nucleation phenomenon in numerous semicrystalline polymers,[49,61] yet the nucleating ability of MWCNTs has not been explained clearly. Most of the authors believe that on polymer/CNTs interaction phase, the CNT helps to reduce energy barrier for nucleation of polymer.

WAXD Analysis

WAXD was used to investigate the crystalline structure of PPCP and PPCP/MWCNT nanocomposites. Figure 11 showed WAXD patterns of PPCP, MWCNT, and PPCP/MWCNT nanocomposites. In this the strong peaks displayed at 2θ (degree)—14, 16.70, 18.73, and 25.36 correspond to L (110), L (040), L (130), and L (060) planes.[62] The planes can be seen in the integrated XRD intensity of PPCP/MWCNT nanocomposites, manifesting the existence of α-crystalline phase. According to XRD traces, the α-crystalline phase (monoclinic crystallization system) and peak position of PPCP in PPCP/MWCNT nanocomposites did

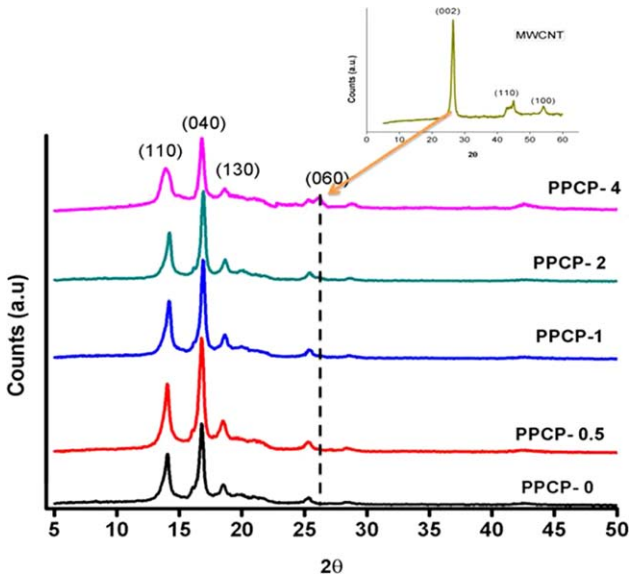

Figure 11. Crystalline morphology of PPCP and PPCP nanocomposites after 8 min of annealing time: (a) PPCP-0, (b) PPCP-0.5, (c) PPCP-1, (d) PPCP-2, and (e) PPCP-4. [Color figure can be viewed in the online issue, which is available at wileyonlinelibrary.com.]

not show any changes upon addition of MWCNTs. XRD pattern of MWCNT show a sharp peak centered at 2θ value of 26° which corresponds to L (002) planes. Two more characteristic peaks were also observed at 2θ value of 43° and 54° which correspond to the diffraction planes of L (101) and L (100), respectively. Presence of this peak may be because of graphitic planes plus a small amount of iron particles encapsulated inside the walls.[63,64] The plane L (060) of nanocomposite PPCP-4 which is corresponding to the plane L (002) of MWCNT confirms the presence of CNTs in the nanocomposites[63] (Figure 11).

CONCLUSIONS

In the studies of crystallization kinetics for PPCP, following conclusion can be drawn:

1. Double fusion endotherms observed in the second heating scans clearly show the formation of imperfect crystals in the presence of MWCNTs which start melting at much lower temperature.
2. Tonset and Peak exothermic temperature of PPCP increased upon incorporation of MWCNTs which confirms that CNT act as poor nucleating agent.
3. The nucleating mechanism of MWCNTs was also supported by Avrami exponent and the time required for 50%crystallization [$t_{1/2}$] which showed a decrease upon incorporation of MWCNTs. The values of Avrami exponent observed in the range 2–3 clearly show two/three dimensional crystal growth.
4. PLM also supported the DSC results as the size of PPCP spherulites decreased in the presence of MWCNTs.
5. Faster crystallization of PPCP in presence of MWCNTs was further supported by the lower values of Kg (4.72×10^5 deg^2) and σe (92.1 erg cm^{-2}). The values of Kg and σe calculated from secondary nucleation theory for PPCP/MWCNT composites showed decreasing trend with increasing MWCNT content indicating that addition of MWCNTs reduced the work required to create a new surface for crystallization and lead to the faster crystallization.
6. X-ray diffraction results indicated that the PPCP have only α form of crystalline structure and incorporation of MWCNTs did not change any crystal structure.

ACKNOWLEDGMENTS

The authors acknowledge R.B. Mathur at National Physical Laboratory, New Delhi, for extending facilities used for MWCNTs synthesis and for the preparation of nanocomposites.

REFERENCES

1. Guidetti, G. P.; Busi, P.; Giulianelli, I.; Zannetti, R. *Eur. Polym. J.* **1983**, *19*, 757.
2. Galli, P.; Haylock, J. C.; Simonazzi, T. In Polypropylene Structure, Blends and composites; Karger-Kocsis, J., Ed.; Springer: Netherlands, **1995**; Chapter 1.
3. Kontopoulou, M.; Wang, W.; Gopakumar, T. G.; Cheung, C. *Polymers* **2003**, *44*, 7495.
4. Starke, J. U.; Michler, G. H.; Grellmann, W.; Seidler, S.; Gahleitner, M.; Fiebig, J.; Nezbedova, E. *Polymers* **1998**, *39*, 75.
5. Fan, Z.-q.; Zhang, Y.-q.; Xu, J.-t.; Wang, H.-t.; Feng, L.-x. *Polymers* **2001**, *42*, 5559.
6. Hoffman, J. D.; Lauritzen, J. I., Jr. *J. Res. Natl. Bur. Stand.* **1961**, Sect. A 65A, 297.
7. Hoffman, J. D. *Polymers* **1983**, *24*, 3.
8. Huang, J.-W. *Polym. Eng. Sci.* **2009**, *49*, 1855.
9. Huang, J.-M.; Ju, M.-Y.; Chu, P.; Chang, F.-C. *J. Polym. Res.* **1999**, *6*, 259.
10. Supaphol, P.; Apiwanthanakorn, N.; Krutphun, P. *Polym. Test.* **2007**, *26*, 985.
11. Wu, T.-M.; Chen, E.-C. *Polym. Eng. Sci.* **2006**, *46*, 1309.
12. Gupta, A.; Choudhary, V. J. *Therm. Anal. Calorim.* **2013**, 1.
13. Ishikawa, H.; Fudetani, S.; Hirohashi, M. *Appl. Surf. Sci.* **2001**, *178*, 56.
14. Kracke, B.; Damaschke, B. *Appl. Phys. Lett.* **2000**, *77*, 361.
15. Ruiz, F.; Sun, W. D.; Pollak, F. H.; Venkatraman, C. *Appl. Phys. Lett.* **1998**, *73*, 1802.
16. Choi, E. S.; Brooks, J. S.; Eaton, D. L.; Al-Haik, M. S.; Hussaini, M. Y.; Garmestani, H.; Li, D.; Dahmen, K. *J. Appl. Phys.* **2003**, *94*, 6034.
17. Coleman, J. N.; Cadek, M.; Blake, R.; Nicolosi, V.; Ryan, K. P.; Belton, C.; Fonseca, A.; Nagy, J. B.; Gun'ko, Y. K.; Blau, W. *J. Adv. Funct. Mater.* **2004**, *14*, 791.
18. Coleman, J. N.; Cadek, M.; Ryan, K. P.; Fonseca, A.; Nagy, J. B.; Blau, W. J.; Ferreira, M. S. *Polymers* **2006**, *47*, 8556.
19. Gorrasi, G.; Di Lieto, R.; Patimo, G.; De Pasquale, S.; Sorrentino, A. *Polymers* **2011**, *52*, 1124.
20. Logakis, E.; Pandis, C.; Peoglos, V.; Pissis, P.; Stergiou, C.; Pionteck, J.; Pötschke, P.; Mičušík, M.; Omastová, M. *J. Polym. Sci. Part B: Polym. Phys.* **2009**, *47*, 764.

21. Logakis, E.; Pollatos, E.; Pandis, C.; Peoglos, V.; Zuburtikudis, I.; Delides, C. G.; Vatalis, A.; Gjoka, M.; Syskakis, E.; Viras, K.; Pissis, P. *Compos. Sci. Technol.* **2010**, *70*, 328.
22. Zhang, S.; Minus, M. L.; Zhu, L.; Wong, C.-P.; Kumar, S. *Polymers* **2008**, *49*, 1356.
23. Li, J.; Fang, Z.; Tong, L.; Gu, A.; Liu, F. *Eur. Polym. J.* **2006**, *42*, 3230.
24. Manchado, M. A. L.; Valentini, L.; Biagiotti, J.; Kenny, J. M. *Carbon* **2005**, *43*, 1499.
25. Sandler, J. K. W.; Pegel, S.; Cadek, M.; Gojny, F.; van Es, M.; Lohmar, J.; Blau, W. J.; Schulte, K.; Windle, A. H.; Shaffer, M. S. P. *Polymers* **2004**, *45*, 2001.
26. Grady, B. P.; Pompeo, F.; Shambaugh, R. L.; Resasco, D. E. *J. Phys. Chem. B* **2002**, *106*, 5852.
27. Reyes-de Vaaben, S.; Aguilar, A.; Avalos, F.; Ramos-de Valle, L. F. *J. Therm. Anal. Calorim.* **2008**, *93*, 947.
28. Jin, J.; Song, M.; Pan, F. *Thermochim. Acta* **2007**, *456*, 25.
29. Díez-Pascual, A. M.; Naffakh, M.; Gómez, M. A.; Marco, C.; Ellis, G.; Martínez, M. T.; Ansón, A.; González-Domínguez, J. M.; Martínez-Rubi, Y.; Simard, B. *Carbon* **2009**, *47*, 3079.
30. Gupta, A.; Choudhary, V. *Macromol. Symp.* **2010**, *290*, 56.
31. Supaphol, P. *Thermochim. Acta* **2001**, *370*, 37.
32. Nandi, S.; Ghosh, A. K. *J. Polym. Res.* **2007**, *14*, 387.
33. Supaphol, P. *J. Appl. Polym. Sci.* **2000**, *79*, 1603.
34. Seo, M.-K.; Lee, J.-R.; Park, S.-J. *Mater. Sci. Eng. A.* **2005**, *404*, 79.
35. Supaphol, P.; Spruiell, J. E. *Polymers* **2001**, *42*, 699.
36. Grady, B. P.; Pompeo, F.; Shambaugh, R. L.; Resasco, D. E. *J. Phys. Chem. B* **2002**, *106*, 5852.
37. Menyhárd, A.; Dora, G.; Horváth, Z.; Faludi, G.; Varga, J. J. *Therm. Anal. Calorim.* **2012**, *108*, 613.
38. Ferreira, C. I.; Dal Castel, C.; Oviedo, M. A. S.; Mauler, R. S. *Thermochim. Acta* **2013**, *553*, 40.
39. Mathur, R. B.; Chatterjee, S.; Singh, B. P. *Compos. Sci. Technol.* **2008**, *68*, 1608.
40. Olalde, B.; Aizpurua, J. M.; Garcia, A.; Bustero, I.; Obieta, I.; Jurado, M. J. *J. Phys. Chem. C* **2008**, *112*, 10663.
41. Gupta, A.; Choudhary, V. *J. Appl. Polym. Sci.* **2012**, *123*, 1548.
42. Pyda, M.; Boller, A.; Grebowicz, J.; Chuah, H.; Lebedev, B. V.; Wunderlich, B. *J. Polym. Sci. Part B: Polym. Phys.* **1998**, *36*, 2499.
43. Cho, K.; Li, F.; Choi, J. *Polymers* **1999**, *40*, 1719.
44. Medellín-Rodríguez, F. J.; Mata-Padilla, M.; Sánchez-Valdes, S.; Vega-Díaz, S.; Dávalos-Montoya, O. *J. Polym. Sci. Part B: Polym. Phys.* **2008**, *46*, 2188.
45. Sahin, S.; Yayla, P. *Polym. Test.* **2005**, *24*, 1012.
46. He, Y.; Fan, Z.; Hu, Y.; Wu, T.; Wei, J.; Li, S. *Eur. Polym. J.* **2007**, *43*, 4431.
47. Trivijitkasem, S.; Timsorn, K.; Kasetsart, J. *Nat. Sci.* **2009**, *43*, 347.
48. Kim, S. H.; Park, S. W.; Gil, E. S. *J. Appl. Polym. Sci.* **1998**, *67*, 1383.
49. Zhou, Z.; Wang, S.; Lu, L.; Zhang, Y.; Zhang, Y. *J. Polym. Sci. Part B: Polym. Phys.* **2007**, *45*, 1616.
50. Marco, C.; Naffakh, M.; Gómez, M. A.; Santoro, G.; Ellis, G. *Polym. Compos.* **2011**, *32*, 324.
51. Hannay, N. B., Ed. Treatise on Solid State Chemistry, Vol. 3: Crystalline and Noncrystalline Solids; Plenum Press: New York, **1976**.
52. Wu, P.-L.; Woo, E. M. *J. Polym. Sci. Part B: Polym. Phys.* **2002**, *40*, 1571.
53. Flory, P. J.; Vrij, A. *J. Am. Chem. Soc.* **1963**, *85*, 3548.
54. Marand, H.; Xu, J.; Srinivas, S. *Macromolecules* **1998**, *31*, 8219.
55. Huang, J.; Prasad, A.; Marand, H. *Polymers* **1994**, *35*, 1896.
56. Hoffman, J. D.; Miller, R. L. *Polymers* **1997**, *38*, 3151.
57. Marand, H.; Xu, J.; Srinivas, S. *Macromolecules* **1998**, *31*, 8219.
58. Xu, J.; Srinivas, S.; Marand, H.; Agarwal, P. *Macromolecules* **1998**, *31*, 8230.
59. Naffakh, M.; Martín, Z.; Marco, C.; Gómez, M. A.; Jiménez, I. *Thermochim. Acta* **2008**, *472*, 11.
60. Li, H.; Gao, X.; Tong, Y. *Hecheng Shuzhi Ji Suliao* **2006**, *23*, 28.
61. Bikiaris, D. *Materials* **2010**, *3*, 2884.
62. Xie, L.; Ziegmann, G. *J. Alloys Compd.* **2011**, *509*, 226.
63. Saini, P.; Choudhary, V.; Singh, B. P.; Mathur, R. B.; Dhawan, S. K. *Mater. Chem. Phys.* **2009**, *113*, 919.
64. Singh, B. P.; Prabha, S. P.; Saini, P.; Gupta, T.; Garg, P.; Kumar, G.; Pande, I.; Pande, S.; Seth, R. K.; Dhawan, S. K.; Mathur, R. B. *J. Nanopart Res.* **2011**, *13*, 7065.